Inorganic Chemistry

Article

pubs.acs.org/IC

Synthesis, Structure, and Magnetism of a Family of Heterometallic $\{Cu_2Ln_7\}$ and $\{Cu_4Ln_{12}\}$ (Ln = Gd, Tb, and Dy) Complexes: The Gd Analogues Exhibiting a Large Magnetocaloric Effect

Stuart K. Langley,[†] Boujemaa Moubaraki,[†] Corrado Tomasi,[‡,§] Marco Evangelisti,*[,§] Euan K. Brechin,[⊥] and Keith S. Murray*[,†]

[†]School of Chemistry, Monash University, Clayton, Victoria 3800, Australia

[‡]I.E.N.I. C.N.R., Unit of Lecco, C.so Promessi Sposi 29, 23900 Lecco, Italy

[§]Departamento de Física de la Materia Condensada and Instituto de Ciencia de Materiales de Aragón, CSIC−Universidad de Zaragoza, 50009 Zaragoza, Spain

[⊥]EaStCHEM School of Chemistry, The University of Edinburgh, David Brewster Road, Edinburgh, EH9 3FJ, U.K.

Supporting Information

ABSTRACT: The syntheses, structures, and magnetic properties of two heterometallic Cu^{II}−Ln^{III} (Ln^{III} = Gd, Tb, and Dy) families, utilizing triethanolamine and carboxylate ligands, are reported. The first structural motif displays a nonanuclear $\{Cu^{II}_2Ln^{III}_7\}$ metallic core, while the second reveals a hexadecanuclear $\{Cu^{II}_4Ln^{III}_{12}\}$ core. The differing nuclearities of the two families stem from the choice of carboxylic acid used in the synthesis. Magnetic studies show that the most impressive features are displayed by the $\{Cu^{II}_2Gd^{III}_7\}$ and $\{Cu^{II}_4Gd^{III}_{12}\}$ complexes, which display a large magnetocaloric effect, with entropy changes $-\Delta S_m$ = 34.6 and 33.0 J kg^{-1} K^{-1} at T = 2.7 and 2.9 K, respectively, for a 9 T applied field change. It is also found that the $\{Cu^{II}_4Dy^{III}_{12}\}$ complex displays single-molecule magnet behavior, with an anisotropy barrier to magnetization reversal of 10.1 K.

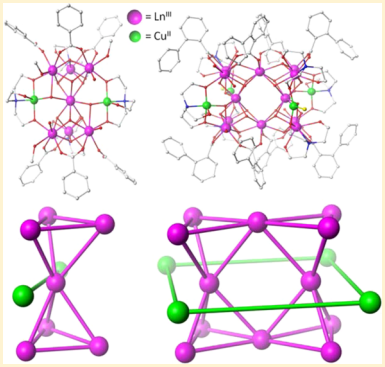

INTRODUCTION

Coordination complexes of transition metal and lanthanide ions continue to attract the attention of many research groups because of their relevance toward molecular magnetism and the many potential applications associated with such molecular magnetic properties.[1] One such focus is the synthesis of single-molecule magnets (SMMs), where 0D nanoscale molecules exhibit slow magnetic relaxation below a blocking temperature, which, in principle, can allow for digital information to be stored at a molecular level.[2] Molecular magnetic complexes have also been shown to display a large magnetocaloric effect (MCE) at cryogenic temperatures and, therefore, can be used as a cooling medium, reducing temperatures below that of liquid helium, a much sought after technology.[3] In recent years the introduction of anisotropic lanthanide ions, such as Tb^{III} and Dy^{III}, has led to significant improvements in SMM properties, with record anisotropy barriers (U_{eff}) and blocking temperatures (T_B) having been reported.[4] Further to this, magnetic refrigeration, which is based on the MCE and measured by the change of the magnetic entropy (ΔS_m) upon application and removal of a magnetic field, has been greatly enhanced via the use of the isotropic Gd^{III} ion in molecular clusters or extended networks.[5] It has been demonstrated that the MCE in molecule-based magnetic compounds can show enormous $-\Delta S_m$ values, larger than those observed for conventional magnetic refrigerants for such low temperatures.[6] The molar magnetic entropy change, i.e., $-\Delta S_m/R$, where R is the gas constant, is maximized at the magnetic entropy value n ln(2S + 1), where n is the number of noninteracting spins with S the spin state value. In an application perspective, the magnetic entropy change is more conveniently expressed per unit mass, and, therefore, $-\Delta S_m$ is inversely proportional to the molecular mass. Indeed, the more effective the magnetic refrigeration, the lighter the relative amount of nonmagnetic elements, such as ligands, which act passively in the MCE. Isotropic metals are also desirable, as anisotropic systems retain magnetic order in zero-external field, thus limiting the entropy change. It was noted some decades ago that Cu^{II}−Gd^{III} interactions are generally weak and ferromagnetic, leading to a large ground spin value,[7] with close low-lying spin states (which enhance the field dependence of the MCE) and with the ions being isotropic, thus fitting the requirements for a large MCE.[3a] With this in mind we previously reported a $[Cu^{II}_5Gd^{III}_4O_2(OMe)_4(teaH)_4(O_2CC(CH_3)_3)_2(NO_3)_4]$ complex that possessed a considerable MCE, with a $-\Delta S_m$ value of 31 J kg^{-1} K^{-1} for $\mu_0\Delta H$ = 9 T at 3 K.[8] The anisotropic analogues $\{Cu^{II}_5Ln^{III}_4\}$ (Ln = Tb, Dy, and Ho) were also

Received: September 29, 2014
Published: November 19, 2014

   dx.doi.org/10.1021/ic5023467 | Inorg. Chem. 2014, 53, 13154−13161

reported,[9] and each displayed SMM behavior. We have therefore extended this heterometallic 3d−4f work, looking at both anisotropic and isotropic Cu^{II}−Ln^{III} coordination complexes.

The synthesis of the above-mentioned isostructural heterometallic $\{Cu^{II}_5Ln^{III}_4\}$ family involved the use of the versatile pro-ligand triethanolamine ($teaH_3$), which has commonly been used for the stabilization of polynuclear metal complexes.[10] The synthetic strategy followed a self-assembled, bottom-up approach, where it has been shown that small changes in the reaction matrix can have profound consequences on the identity of the final product.[11] Here we report an extension of our initial Cu^{II}−Ln^{III} work revealing that simple variations of the copper and lanthanide salts, as well as the carboxylate coligand, resulted in two new high-nuclearity Cu^{II}−Ln^{III} species. The complexes presented are of general formulas $[Cu^{II}_2Gd^{III}_7(OH)_{10}(teaH)_2(teaH_3)_2(O_2CPh)_6(MeOH)_3(H_2O)_3](Cl)_5\cdot 6H_2O$ (**1**), $[Cu^{II}_2Ln^{III}_7(OH)_{10}(teaH)_2(teaH_3)_2(O_2CPh)_6(MeOH)_2(H_2O)_4](Cl)_5\cdot xH_2O$ {Tb (**2**) and Dy (**3**), x = 5 or 6}, and $[Cu^{II}_4Ln^{III}_{12}(OH)_{20}(teaH)_2(teaH_2)_4(O_2CPh\text{-}2\text{-}Ph)_8(H_2O)_6Cl_2](Cl)_6\cdot 2MeOH\cdot 4H_2O$ {Ln = Gd (**4**), Tb (**5**), and Dy (**6**)}. The synthesis and magnetic properties are reported, with an evaluation of the MCE for the isotropic Gd^{III} containing complexes **1** and **4**, resulting in large $-\Delta S_m$ values. The relaxation dynamics are probed for the anisotropic ions, with compound **6** displaying clear SMM behavior.

EXPERIMENTAL SECTION

General Information. All reactions were carried out under aerobic conditions. Chemicals and solvents were obtained from commercial sources and used without further purification. Elemental analyses (CHN) were carried out by Campbell Microanalytical Laboratory, University of Otago, Dunedin, New Zealand.

*$[Cu^{II}_2Gd^{III}_7(OH)_{10}(teaH)_2(teaH_3)_2(O_2CPh)_6(MeOH)_3(H_2O)_3](Cl)_5\cdot 6H_2O$ (**1**).* $CuCl_2\cdot 2H_2O$ (0.05 g, 0.29 mmol) and $GdCl_3\cdot 6H_2O$ (0.37 g, 1.0 mmol) were dissolved in 20 mL of CH_2Cl_2/MeOH (17:3) followed by the addition of triethanolamine (0.07 mL, 0.50 mmol), benzoic acid (0.1 g, 0.80 mmol), and triethylamine (0.49 mL, 3.5 mmol) to give a deep blue solution. This was stirred for 4 h, after which the solution was layered with diethyl ether. After 2−3 days, blue crystals of **1** had formed. Yield: 39.2%. Anal. Calcd (found) for **1**·$6H_2O$: $Cu_2Gd_7C_{69}H_{122}O_{46}N_4Cl_5$: C, 26.31 (26.60); H, 3.90 (4.21); N, 1.78 (2.01).

*$[Cu^{II}_2Tb^{III}_7(OH)_{10}(teaH)_2(teaH_3)_2(O_2CPh)_6(MeOH)_2(H_2O)_4](Cl)_5\cdot 6H_2O$ (**2**).* As in **1** but $TbCl_3\cdot 6H_2O$ (0.37 g, 1.0 mmol) was used in place of $GdCl_3\cdot 6H_2O$. Yield: 46.2%. Anal. Calcd (found) for **2**·$6H_2O$: $Cu_2Tb_7C_{68}H_{120}O_{46}N_4Cl_5$: C, 25.96 (26.20); H, 3.84 (4.19); N, 1.78 (2.09).

*$[Cu^{II}_2Dy^{III}_7(OH)_{10}(teaH)_2(teaH_3)_2(O_2CPh)_6(MeOH)_2(H_2O)_4](Cl)_5\cdot 5H_2O$ (**3**).* As in **1** but $DyCl_3\cdot 6H_2O$ (0.38 g, 1.0 mmol) was used in place of $GdCl_3\cdot 6H_2O$. Yield: 52.6%. Anal. Calcd (found) for **3**·$5H_2O$: $Cu_2Dy_7C_{68}H_{118}O_{45}N_4Cl_5$: C, 25.90 (26.15); H, 3.77 (4.04); N, 1.78 (1.83).

*$[Cu^{II}_4Gd^{III}_{12}(OH)_{20}(teaH)_2(teaH_2)_4(O_2CPh\text{-}2\text{-}Ph)_8(H_2O)_6Cl_2](Cl)_6\cdot 2MeOH\cdot 4H_2O$ (**4**).* $CuCl_2\cdot 2H_2O$ (0.07 g, 0.4 mmol) and $GdCl_3\cdot 6H_2O$ (0.37 g, 1.0 mmol) were dissolved in 20 mL of CH_2Cl_2/MeOH (16:4), followed by the addition of triethanolamine (0.07 mL, 0.50 mmol), 2-biphenylcarboxylic acid (0.16 g, 0.80 mmol), and triethylamine (0.28 mL, 2.0 mmol) to give a deep blue solution. This was then stirred for 4 h, after which time the solution was layered with diethyl ether. After 1−2 days, blue crystals of **4** had formed. Yield: 29.2%. Anal. Calcd (found) for **4**·$2MeOH\cdot 4H_2O$: $Cu_4Gd_{12}C_{142}H_{202}O_{66}N_6Cl_8$: C, 31.16 (31.40); H, 3.72 (4.01); N, 1.53 (1.59).

*$[Cu^{II}_4Tb^{III}_{12}(OH)_{20}(teaH)_2(teaH_2)_4(O_2CPh\text{-}2\text{-}Ph)_8(H_2O)_6Cl_2](Cl)_6\cdot 2MeOH\cdot 4H_2O$ (**5**).* As in **4** but $TbCl_3\cdot 6H_2O$ (0.37 g, 1 mmol) was used in place of $GdCl_3\cdot 6H_2O$. Yield: 32.5%. Anal. Calcd (found) for **5**·$2MeOH\cdot 4H_2O$: $Cu_4Tb_{12}C_{142}H_{202}O_{66}N_6Cl_8$: C, 31.04 (31.20); H, 3.71 (3.49); N, 1.53 (1.39).

*$[Cu^{II}_4Dy^{III}_{12}(OH)_{20}(teaH)_2(teaH_2)_4(O_2CPh\text{-}2\text{-}Ph)_8(H_2O)_6Cl_2](Cl)_6\cdot 2MeOH\cdot 4H_2O$ (**6**).* As in **4** but $DyCl_3\cdot 6H_2O$ (0.38 g, 1 mmol) was used in place of $GdCl_3\cdot 6H_2O$. Yield: 36.4%. Anal. Calcd (found) for **6**·$2MeOH\cdot 4H_2O$: $Cu_4Dy_{12}C_{142}H_{202}O_{66}N_6Cl_8$: C, 30.80 (30.55); H, 3.68 (3.62); N, 1.52 (1.73).

Physical Measurements. *X-ray Crystallography.* X-ray crystallographic measurements were performed at 100(2) K for **1**−**6** at the Australian synchrotron MX1 beamline. The data collection and integration were performed within Blu-Ice[12] and XDS[13] software programs. Compounds **1**−**6** were solved by direct methods (SHELXS-97) and refined (SHELXL-97) by full matrix least-squares on all F^2 data.[14] Crystallographic data and refinement parameters are summarized in Table S1. Crystallographic details are available in CIF format. CCDC numbers 1025930−1025935 (**1**−**6**). These data can be obtained free of charge from the Cambridge Crystallographic Data Centre via www.ccdc.cam.ac.uk/data_request/cif.

Magnetic Measurements. The magnetic susceptibility measurements were carried out on a Quantum Design SQUID magnetometer MPMS-XL 7 operating between 1.8 and 300 K for dc-applied fields ranging from 0 to 5 T. Microcrystalline samples were dispersed in Vaseline in order to avoid torquing of the crystallites. The sample mulls were contained in a calibrated gelatin capsule held at the center of a drinking straw that was fixed at the end of the sample rod. Alternating current (ac) susceptibility measurements were carried out under an oscillating ac field of 3.5 Oe and frequencies ranging from 0.1 to 1500 Hz.

Heat Capacity Measurements. The heat capacity measurements were carried out for temperatures down to 0.3 K by using a Quantum Design 14T-PPMS, equipped with a ^{3}He cryostat. The experiments were performed on thin pressed pellets (ca. 1 mg) of a polycrystalline sample, thermalized by ca. 0.2 mg of Apiezon N grease, whose contribution was subtracted by using a phenomenonological expression.

RESULTS AND DISCUSSION

Synthesis. The synthesis of the previously reported $[Cu^{II}_5Ln^{III}_4O_2(OMe)_4(teaH)_4(O_2CC(CH_3)_3)_2(NO_3)_4]$ (Ln = Gd, Tb, Dy, and Ho) family of complexes involved the reaction of $Cu(NO_3)_2\cdot 2H_2O$ and $Ln(NO_3)_3\cdot 6H_2O$ with $teaH_3$, pivalic acid, and triethylamine in methanol.[8] Using the above synthetic reagents as a starting point, reactions performed in the present study utilized hydrated metal chloride salts, in place of the nitrate salts, as it was noted that nitrate anions influenced the formation of the $\{Cu^{II}_5Ln^{III}_4\}$ complexes. Using this variation, we found that a new nonanuclear family of metallic core type $\{Cu^{II}_2Ln^{III}_7\}$ could be isolated, all of which were crystallized from the specific CH_2Cl_2/MeOH solvent ratio of 17:3. While the reaction with pivalic acid was found to be successful, the use of benzoic acid, which is reported here, resulted in the same metallic core structure and was the preferred acid due to higher yields and easier purification of the product. Upon variation of the lanthanide ion, three isostructural products were isolated, with the compounds having the general formula $[Cu^{II}_2Ln^{III}_7(OH)_{10}(teaH)_2(teaH_3)_2(O_2CPh)_6(MeOH)_n(H_2O)_m](Cl)_5\cdot xH_2O$ {Ln = Gd (**1**), Tb (**2**), and Dy (**3**), n = 2 or 3, m = 4 or 3, and x = 5 or 6}. Replacement of benzoic acid by the more sterically hindered 2-biphenylcarboxylic acid resulted in the formation of a new higher nuclearity motif of core type $\{Cu^{II}_4Ln^{III}_{12}\}$, which has structural similarities to **1**−**3**. Indeed, it is often found that the use of bulky carboxylic acids over less sterically demanding ones enforces structural rearrangements in polynuclear chemistry.[10a,15] Again, three isostructural products were isolated from CH_2Cl_2/MeOH

dx.doi.org/10.1021/ic5023467 | Inorg. Chem. 2014, 53, 13154−13161

(16:4), with the compounds displaying the general formula $[Cu^{II}_4Ln^{III}_{12}(OH)_{20}(teaH)_2(teaH_2)_4(O_2CPh\text{-}2\text{-}Ph)_8(H_2O)_6Cl_2](Cl)_6\cdot 2MeOH\cdot 4H_2O$ {Ln = Gd (**1**), Tb (**2**), and Dy (**3**)}. We can see, therefore, that very simple chemical modifications lead to structurally desirable and novel 3d-4f motifs, these being easily accessible under mild reaction conditions and employing common starting materials.

Structural Descriptions. *$[Cu^{II}_2Gd^{III}_7(OH)_{10}(teaH)_2(teaH_3)_2(O_2CPh)_6(MeOH)_3(H_2O)_3](Cl)_5\cdot 6H_2O$ (**1**) and $[Cu^{II}_2Ln^{III}_7(OH)_{10}(teaH)_2(teaH_3)_2(O_2CPh)_6(MeOH)_2(H_2O)_4](Cl)_5\cdot xH_2O$ {Ln = Tb (**2**) and Dy (**3**), x = 5 or 6}.* Crystals suitable for X-ray diffraction were grown from diffusion of diethyl ether into the CH_2Cl_2/MeOH solvent mixture, with each complex found to crystallize in the orthorhombic space group $Pca2_1$. The asymmetric unit consists of the entire cluster, five chloride counterions, with several water molecules also found in the lattice. The complexes are essentially isostructural, one difference however being a terminal MeOH having replaced a terminal H_2O molecule for **1** compared to **2** and **3**. For the sake of brevity only a structural description of **1** is given. Compound **1** (Figure 1) is a nonanuclear heterometallic complex,

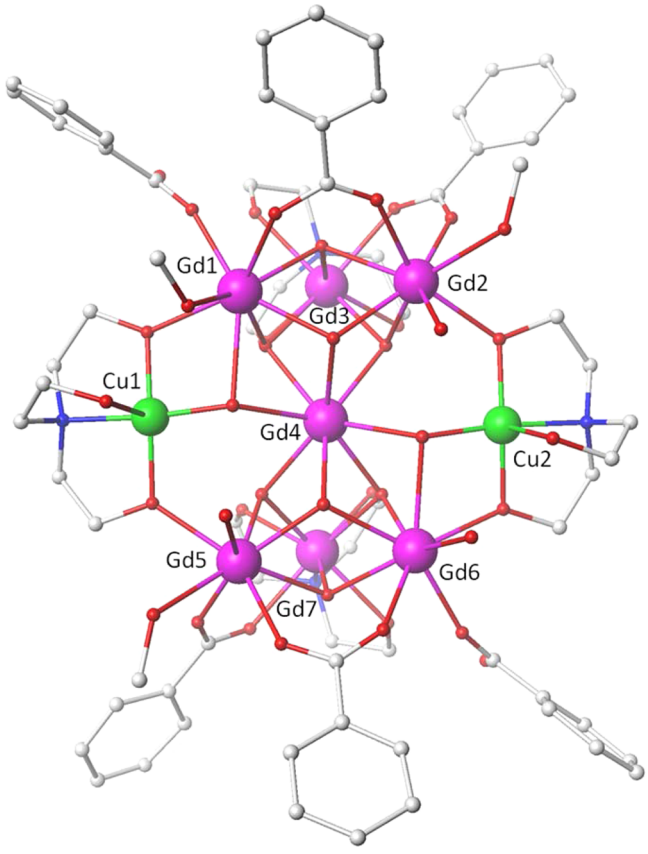

Figure 1. Molecular structure of the cation of complex **1** in the crystal. The chloride anions, solvent, and H atoms are omitted for clarity. Color scheme: Cu^{II}, green; Ln^{III}, purple; O, red; N, blue; C, light gray.

consisting of two Cu^{II} and seven Gd^{III} ions. The metallic core can be described as two cubanes (Gd1−Gd7), which share a common vertex (Gd4), with two capping Cu^{II} ions (Cu1 and Cu2). The inorganic core is stabilized via 10 μ_3 bridging hydroxides. Eight of these are found at the vertices of the cubanes, resulting in two $\{Gd^{III}_4(\mu_3\text{-}OH)_4\}^{8+}$ fragments. The final two hydroxide ligands bridge from {Gd4 and Gd6} and {Gd4 and Gd1} to Cu2 and Cu1, respectively. The remaining coordination sites are occupied by various bridging and terminal organic ligands. These consist of two doubly deprotonated $[teaH]^{2-}$, two $teaH_3$, and six benzoate ligands, with three H_2O and three MeOH molecules. The two doubly deprotonated $[teaH]^{2-}$ ligands are bridging, and both display the μ_3:η^2:η^2:η^1:η^1 bonding mode. Each coordinate to a Cu^{II} ion via the N atom, with two of the O atoms bridging the Cu^{II} to a Gd^{III} ion. The third protonated alcohol arm forms a weak axial contact to the Cu^{II} ion, with a bond distance of 2.48−2.53 Å. The two $teaH_3$ ligands chelate via all donor [N,O,O,O] atoms to Gd3 and Gd7, respectively. Four of the benzoate ligands bridge in the usual *syn,syn* bonding mode, each bridging two Gd^{III} ions across the edges of the cubanes. The final two benzoates lie terminal, coordinating to Gd1 and Gd6 via a single O atom. The coordination sites of the Gd^{III} ions are completed by three terminal MeOH and three terminal water ligands. All of the Gd^{III} ions are eight coordinate, with distorted square-antiprismatic geometries. The Cu^{II} ions are five coordinate (including the long O atom contact), with a square-pyramidal geometry. The average Gd−$L_{N,O}$ and Cu−$L_{N,O}$ bond distances are 2.41 and 2.04 Å, respectively. The average (closest) Gd···Gd, Cu···Gd, and Cu···Cu contacts are 3.83, 3.72, and 7.84 Å, respectively. Intermolecular interactions are dominated by parallel displaced aromatic π−π interactions (centroid to centroid distance 4.1 Å) and edge to face configurations between the benzoate ligands (Figure S1).

*$[Cu^{II}_4Gd^{III}_{12}(OH)_{20}(teaH)_2(teaH_2)_4(O_2CPh\text{-}2\text{-}Ph)_8(H_2O)_6Cl_2](Cl)_6\cdot 2MeOH\cdot 4H_2O$ {Ln = Gd (**4**), Tb (**5**), and Dy (**6**)}.* Crystals suitable for X-ray diffraction were grown by layering the CH_2Cl_2/MeOH solvent mixture with diethyl ether, with each complex crystallizing in the triclinic space group $P\bar{1}$. The asymmetric unit consists of half the cluster, which lies upon an inversion center, with six chloride counterions and several solvent water and MeOH molecules. Again, each complex is isostructural, and a description of **4** is given. Compound **4** (Figure 2, top) is a heterometallic hexadecanuclear complex consisting of four Cu^{II} and 12 Gd^{III} ions. The metallic core is similar to that observed for compounds **1**−**3** and can be described as four vertex-sharing cubanes (Gd1−Gd6 and symmetry-generated atoms), with four capping Cu^{II} ions (Cu1 and Cu2 and symmetry-generated atoms). The common vertices are provided by Gd3, Gd5, Gd3′, and Gd5′, with the four cubanes, overall, forming a single fused structure. The structural similarity between **4** and **1** can be seen in Figure 2, bottom, with **1** being a "building block" from which **4** is built. The arrangement of the Gd^{III} ions displayed for **4** has been observed previously for $\{M^{II}_8Gd^{III}_4\}$ (M^{II} = Zn, Ni, and Cu) complexes, reported by some of us.[16] While these complexes have a much smaller gadolinium content, they are relevant toward this study, as their MCE values were evaluated. The maximum entropy change, for $\mu_0\Delta H$ = 7 T, of 18.0, 14.6, and 22.0 J kg^{-1} K^{-1} for the Zn, Cu, and Ni complexes, respectively, was reported. The key point of the study, however, highlighted the negative effect that antiferromagnetic exchange has on the MCE. The metallic core arrangement for **4** is stabilized via 20 μ_3 bridging hydroxides, 16 of which are found at the vertices of the cubanes, identical to **1**, with four $\{Gd^{III}_4(\mu_3\text{-}OH)_4\}^{8+}$ fragments found. The remaining four hydroxide ligands bridge Gd5 and Gd5′ and a further Gd^{III} ion to a Cu^{II} ion. Around the periphery of the complex the metallic core is again stabilized by numerous organic bridging and capping ligands. Four $[teaH_2]^-$ and two $[teaH]^{2-}$ ligands display the μ_3: η^2:η^1:η^1:η^1 and μ_3:

dx.doi.org/10.1021/ic5023467 | *Inorg. Chem.* 2014, 53, 13154−13161

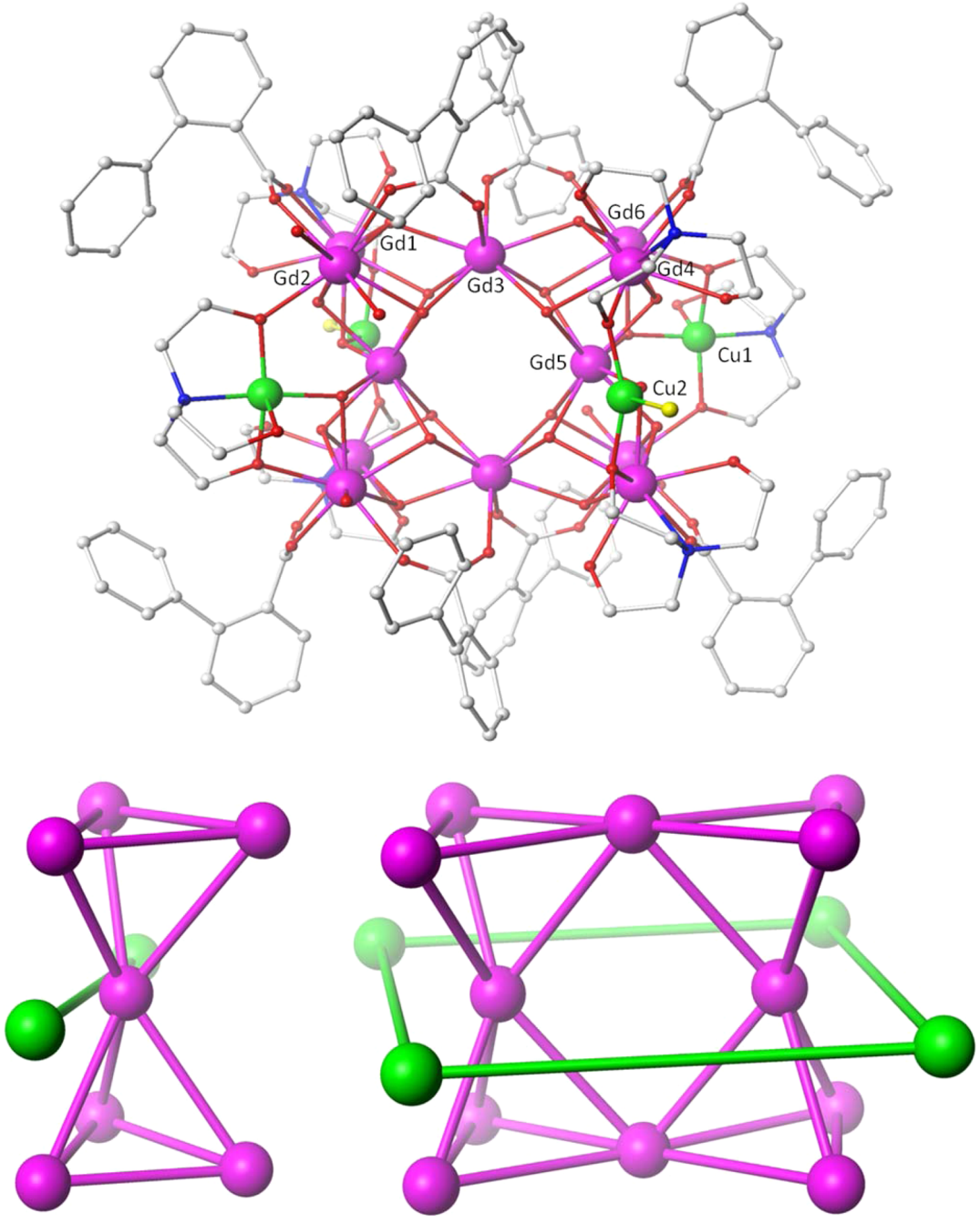

Figure 2. (Top) Molecular structure of the cation of complex **4** in the crystal. The chloride counterions, solvent, and H atoms are omitted for clarity. Color scheme: Cu^{II}, green; Ln^{III}, purple; Cl, yellow; O, red; N, blue; C, light gray. (Bottom) Metal core, highlighting the structural similarity of **1**–**3** (left) to **4**–**6** (right).

$\eta^2{:}\eta^2{:}\eta^1{:}\eta^1$ bridging modes. Eight *syn,syn* carboxylate ligands bridge exclusively to the Gd^{III} ions, while four terminal water and two terminal chloride ions are also found. Eight of the Gd^{III} ions are eight coordinate, while four are nine coordinate, displaying distorted square-antiprismatic and capped square-antiprismatic geometries, respectively. Cu1 and Cu1′ are five coordinate, each with one long axial contact (2.41 Å), and display square-pyramidal geometries. Cu2 and Cu2′ are four coordinate, exhibiting distorted square-planar geometries. The average Gd–$L_{O,N}$ and Cu–$L_{O,N}$ bond lengths are 2.47 and 2.03 Å, respectively. Intermolecular interactions are again dominated by parallel displaced aromatic π–π interactions and edge to face configurations derived from the 2-biphenylcarboxylate ligands (Figure S2).

Magnetic Measurements. Direct Current Magnetic Susceptibility Measurements. In order to probe the magnetic properties, direct current (dc) magnetic susceptibility measurements were performed on polycrystalline samples in the temperature range 2–300 K, with an applied magnetic field of 0.1 T. The $\chi_M T$ (χ_M is the molar magnetic susceptibility) versus T plots for **1**–**3** (Figure 3) reveal room-temperature $\chi_M T$ values of 55.7, 83.4, and 99.5 cm^3 K mol^{-1}, respectively. These values are in good agreement with that expected for two Cu^{II} ($S = 1/2$, $g = 2$) and seven Gd^{III} ($^8S_{7/2}$, $g = 2$), Tb^{III} ($^7F_6$, $g = 3/2$), and Dy^{III} ($^6H_{15/2}$, $g = 4/3$) noninteracting ions of 55.9,

dx.doi.org/10.1021/ic5023467 | *Inorg. Chem.* 2014, 53, 13154–13161

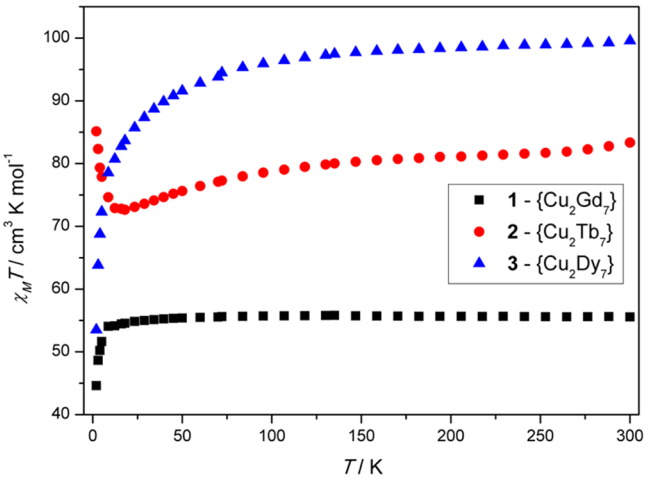

Figure 3. Plots of $\chi_M T$ versus T for compounds **1**–**3** at H = 1000 Oe.

83.5, and 99.9 cm^3 K mol^{-1}, respectively, all indicative of weak magnetic exchange. For compound **1** the $\chi_M T$ values remain constant upon lowering the temperature down to ca. 50 K, with a small decrease observed between 50 and 10 K, before a larger decrease at the lowest temperatures measured. The constant $\chi_M T$ value over the 300–50 K temperature range again indicates weak magnetic exchange, while the decrease at the lowest temperatures suggests overall dominant antiferromagnetic behavior; the latter may also be a result of Zeeman effects. Fits of the data, however, are precluded due to the extremely large matrix dimension needed to perform the calculation. We are therefore unable to quantify the pairwise exchange interactions and determine the overall ground-state and spin energy spectrum for this isotropic system. Compounds **2** and **3** reveal a decline in the $\chi_M T$ product upon reduction of the temperature from 300 K. It is however unclear if weak antiferromagnetic exchange is involved, due to the obscuring nature of the crystal field effects. A small rise below 25 K is, however, observed for **2**, indicative of weak ferromagnetic interactions, whereas a continuous decrease is observed for **3**, suggesting dominant antiferromagnetic exchange overall.

The $\chi_M T$ versus T plots for **4**–**6** (Figure 4) reveal room-temperature $\chi_M T$ values of 95.3, 142.4, and 168.7 cm^3 K mol^{-1}, respectively. These values are again in good agreement with

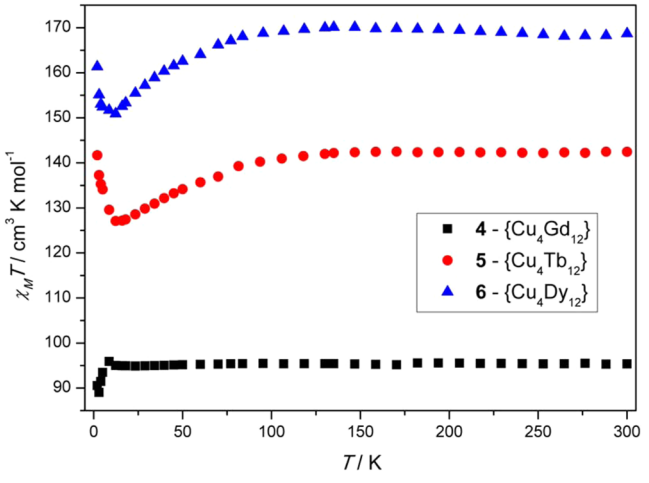

Figure 4. Plots of $\chi_M T$ versus T for compounds **4**–**6** at H_{dc} = 1000 Oe.

that expected for two Cu^{II} (S = 1/2, g = 2) and 12 Gd^{III} ($^8S_{7/2}$, g = 2), Tb^{III} ($^7F_6$, g = 3/2), and Dy^{III} ($^6H_{15/2}$, g = 4/3) noninteracting ions of 96.1, 143.3, and 171.5 cm^3 K mol^{-1}, respectively. Compound **4** displays behavior similar to compound **1**, indicative of weak magnetic exchange. Again, due to the large number of spin states, the sign or magnitude of the pairwise exchange interactions could not be evaluated. At the lowest temperatures, however, there is a hint of an increase in the $\chi_M T$ product at 0.1 T. Measurements performed at smaller fields (0.01 T), in the low-temperature region, further indicate this to be the case (Figure S3) and suggest that ferromagnetic exchange interactions are in play. Compounds **5** and **6** both display a decrease in $\chi_M T$ upon reduction of the temperature, before a clear increase below 15 K is observed. Again it is hard to delineate the nature of the magnetic exchange interactions due to the obscuring effects of the ligand field, which split the ground spin–orbit multiplet on a similar energy scale to the thermal energy available in the system. The very low temperature increase in $\chi_M T$, however, suggests ferromagnetic interactions are present and are the dominant interaction. Similarly to the isotropic systems **1** and **4**, the magnetism of **2**, **3**, **5**, and **6**, which involve ions with an orbital component in their magnetism, is even more complex; again making a qualitative analysis impossible at this time. While a quantitative analysis is not possible, qualitatively one can derive from the temperature-dependent behavior, particularly from the Cu–Gd complexes, that the magnetic exchange interactions found between the ions are weak. From this conclusion, and with the large gadolinium content, compounds **1** and **4** are therefore strong candidates for the observation of a large MCE.

Heat Capacity Measurements. Figure 5 shows the heat capacity (C) collected for polycrystalline samples of **1** and **4**, in the temperature range ~0.3–30 K and applied field values of $\mu_0 H$ = 0, 1, 5, and 9 T. At the higher temperatures, the heat capacity of both compounds is dominated by a nonmagnetic contribution arising from thermal vibrations of the lattice, which can be described by the Debye–Einstein model (dashed lines in Figure 5).[3b] The phonon heat capacity simplifies to a $C/R = aT^3$ dependence at the lowest temperatures, where R is the gas constant and a = 4.3 × 10^{-3} K^{-3} and 1.44 × 10^{-2} K^{-3} for **1** and **4**, respectively. The larger a is, the softer are the low-energy vibration modes,[3b] which are more likely to be present in **4** due to the larger intermolecular mean distances, viz., $(V/Z)^{1/3}$ = 1.41 and 1.68 nm for **1** and **4**, respectively (see crystallographic details in the Supporting Information). The magnetic contribution (C_m) to the heat capacity for both compounds mainly consists of a broad hump, i.e., Schottky heat capacity, which shifts toward higher temperatures on increasing the applied magnetic field (Figure 5). As a comparison with the experimental field-dependent data, we show the contributions (solid lines for $\mu_0 H$ = 5 and 9 T, respectively) that result by summing together the aforementioned phonon heat capacity and Schottky curves arising from the field-split levels of two (four) Cu^{II} and seven (12) Gd^{III} magnetically independent spins for **1** (**4**). Note that the better the agreement, the larger the applied field, which promotes a correspondingly larger decoupling between the individual spin centers. Also note the relatively better agreement for **1** (especially visible by comparing the 3 T curves below 1 K), which denotes a smaller internal field, thus weaker intramolecular exchange interactions, in **1** than in **4**. On lowering the temperature and applied field, the intramolecular exchange interactions result in a net magnetic moment per molecule, which is supposedly larger in

dx.doi.org/10.1021/ic5023467 | Inorg. Chem. 2014, 53, 13154–13161

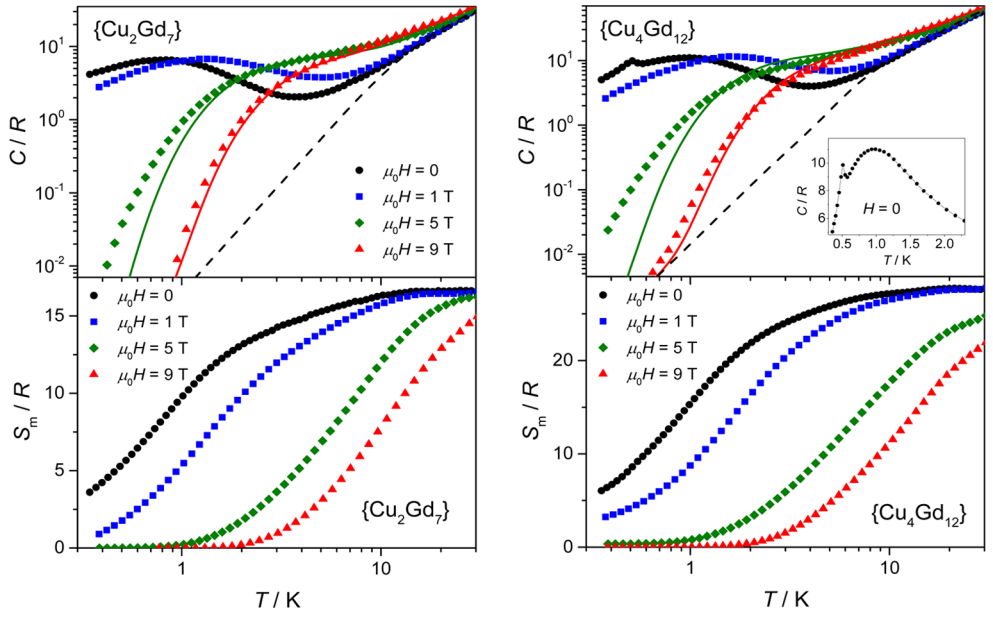

Figure 5. Temperature-dependent heat capacity (top) and magnetic entropy (bottom) plots for **1** (left) and **4** (right) at the indicated applied fields. For comparison, experimental data points are plotted together with the calculated curves: the phonon heat capacity (dashed lines) and the sum of the phonon heat capacity with the Schottky contributions for μ_0H = 5 and 9 T (solid lines). Inset: Experimental zero-field heat capacity for **4** at the lowest temperatures to highlight the magnetic phase transition occurring at T_C = 0.51 K. The solid line just joins the points.

4. Concomitantly, dipole−dipole interactions promote long-range correlations, ultimately driving **4** to a magnetic phase transition at T_C = 0.51 K, as evidenced by the lambda-like peak in the zero-field C (see inset of Figure 5). From the heat capacity, the temperature-dependence of the magnetic entropy is obtained by integration, i.e., $S_m(T) = \int(C_m/T)dT$, and depicted in the bottom panels of Figure 5 for the corresponding applied fields. As expected, S_m/R tends to the maximum entropy value per mole involved at high temperatures, corresponding to two Cu^{II} S = 1/2 and seven Gd^{III} S = 7/2 spins, i.e., 2 × ln(2) + 7 × ln(8) = 15.9 for **1** and four Cu^{II} S = 1/2 and 12 Gd^{III} S = 7/2 spins, i.e., 4 × ln(2) + 12 × ln(8) = 27.7 for **4**. For μ_0H = 0 and 1 T, our experimental blindness for temperatures lower than ca. 0.3 K forced us to add a constant value to the corresponding $S_m(T)$ curves in order to match the limiting value at high temperature (Figure 5).

Evaluation of the MCE. Isothermal magnetization (M) measurements for **1**−**6**, plotted as a function of the magnetic field (H) are shown in Figure 6 (**1** and **4**) and Figures S4−S7 (**2**, **3**, **5**, and **6**).

The magnetization value of 50.5 and 85.2 $N\mu_B$ for **1** and **4** indicates that the largest spin states, which are considerable in magnitude, are accessible at moderate magnetic fields. This situation occurs due to the large number of Gd^{III} ions present and weak magnetic exchange between the ions, which was indicated via the temperature-dependent χ_MT and C plots. As stated, this situation is promising for a large low-temperature MCE, which can be evaluated from the $M(T,H)$ data, shown in Figure 6, by making use of the Maxwell relation; namely, the magnetic entropy change is $\Delta S_m(T) = \int(\partial M/\partial T)\,dH$. The results are shown in Figure 7 for applied field changes $\mu_0\Delta H$ = 1−0 and 5−0 T. A far more complete estimate of $\Delta S_m(T,\Delta H)$ involves the use of the heat capacity data, which we collected for a significantly broader temperature range and up to higher applied fields. From the entropy data in Figure 5, we straightforwardly obtain the $\Delta S_m(T)$ curves that we depict in Figure 7 for $\mu_0\Delta H$ = 1−0, 5−0, and 9−0 T. The very nice

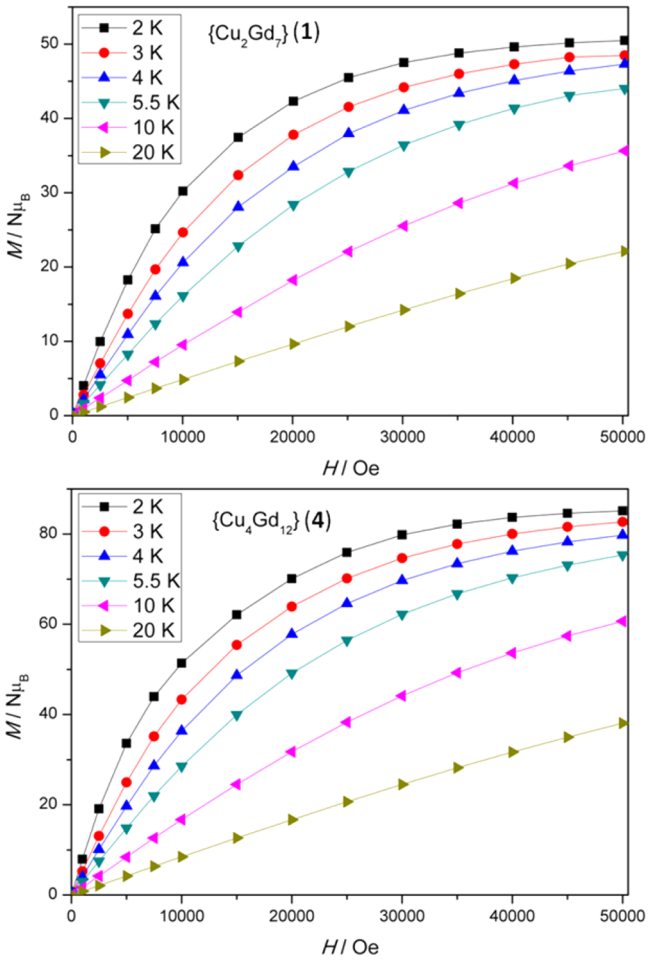

Figure 6. Field-dependent magnetization plots for **1** (left) and **4** (right) at the indicated temperatures. The solid lines just join the points.

dx.doi.org/10.1021/ic5023467 | Inorg. Chem. 2014, 53, 13154−13161

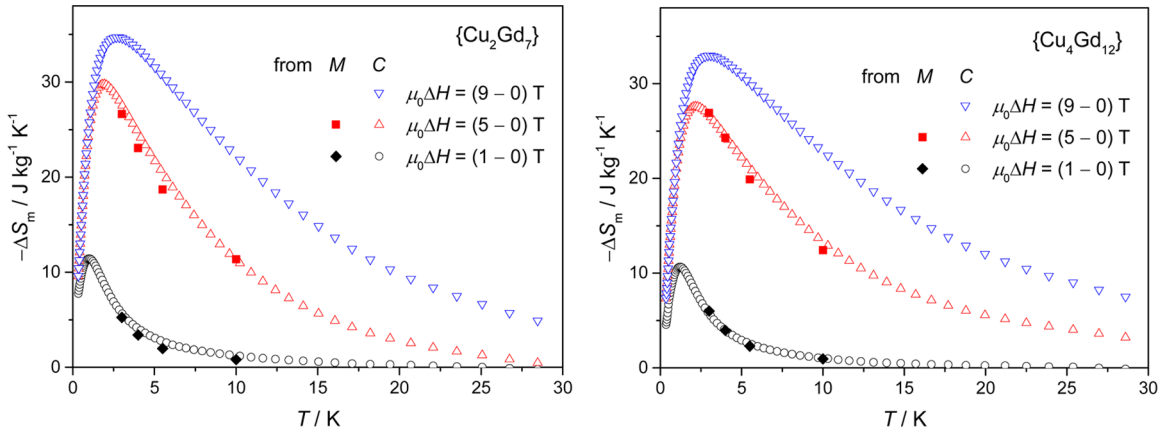

Figure 7. Temperature-dependent magnetic entropy change plots for **1** (left) and **4** (right) at the indicated applied field changes, as obtained from magnetization (Figure 5) and heat capacity (Figure 6) data, as labeled.

agreement with the data obtained from M proves that the aforementioned experimental uncertainty in the low-temperature entropy does not affect the evaluation of the MCE.

When looking at Figure 7, we note that the two compounds have extremely similar $\Delta S_m(T)$ curves for the corresponding applied field values. For the maximum $\mu_0\Delta H$ = 9−0 T, the maximum value of the entropy change is significantly large, achieving $-\Delta S_m$ = 34.6 J kg^{-1} K^{-1} at T = 2.7 K for **1** and $-\Delta S_m$ = 33.0 J kg^{-1} K^{-1} at T = 2.9 K for **4**. The slight difference can be entirely ascribed to the weaker internal field in **1**, as deduced from the heat capacity experiments. Indeed, the weaker the magnetic interactions, the stronger the field-dependence of the $-\Delta S_m(T)$ curves at a lower temperature.[3a] Note that, by coincidence, the different nuclearity [$\{Cu_2Gd_7\}$ and $\{Cu_4Gd_{12}\}$] does not strictly play a role when expressing ΔS_m per unit mass. The full content of the magnetic entropy amounts to 42.1 J kg^{-1} K^{-1} regardless of the compound considered, as can indeed be obtained from the entropy value of 15.9R and molecular mass m = 3136.52 g mol^{-1} in the case of **1** and 27.7R and m = 5473.70 g mol^{-1} in the case of **4**.

The maximum entropy change of 34.6 J kg^{-1} K^{-1} at T = 2.7 K for **1** and $-\Delta S_m$ = 33.0 J kg^{-1} K^{-1} for **4** for a $\mu_0\Delta H$ = 9−0 T compare favorably with reported 0D 3d-4f complexes. They display the largest values for any Cu−Gd system.[8,16,17] Interestingly **4** is significantly greater than the $\{Cu_8Gd_4\}$ example highlighted earlier, with a similar metal topology, which displayed a maximum entropy change of 14.6 J kg^{-1} K^{-1} ($\mu_0\Delta H$ = 7−0 T).[16] This was to be expected due to the greater Gd^{III} content in the sample. It is found that only two 3d-4f complexes display greater entropy changes, these being $\{Gd_{42}Co_{10}\}$ and $\{Gd_{36}Ni_{10}\}$, with values of 41.3 and 36.3 J kg^{-1} K^{-1} for a $\mu_0\Delta H$ = 7−0 T.[18,19]

Alternating Current Magnetic Susceptibility Measurements. The magnetization dynamics were investigated for the anisotropic complexes **2**, **3**, **5**, and **6** by alternating current (ac) susceptibility measurements as a function of temperature and frequency. A 3.5 Oe ac field was employed, with a zero static dc field. No SMM behavior was observed above 1.8 K for the $\{Cu^{II}_2Tb^{III}_7\}$ (**3**) and $\{Cu^{II}_4Tb^{III}_{12}\}$ (**5**) compounds due to the absence of any frequency-dependent out-of-phase (χ_M'') signals (Figures S8 and S9). A nonzero out-of-phase component is observed for $\{Cu^{II}_2Dy^{III}_7\}$ (**4**); however, no maxima are observed (Figure S10). This does not prove SMM behavior, but suggests the possibility of such, with a small energy barrier to magnetic reorientation. Clear maxima are observed, however, for $\{Cu^{II}_4Dy^{III}_{12}\}$ (**6**), indicating slow relaxation of the magnetization and SMM behavior (Figure 8).

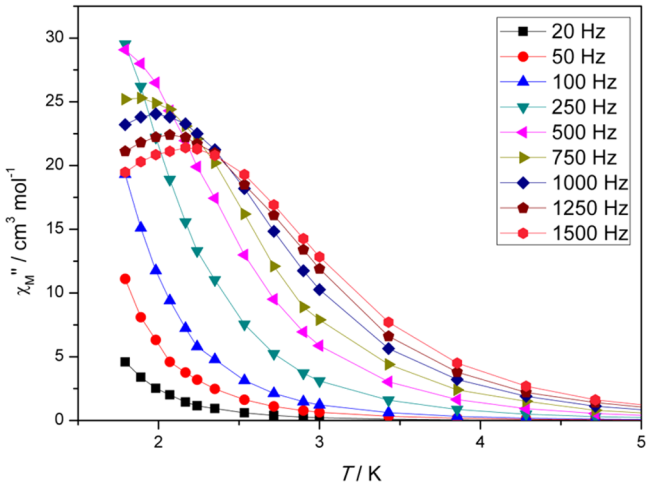

Figure 8. Plot of χ_M'' versus T at the frequencies indicated for **6** with H = 0.

From these data, the relaxation times ($\tau = (2\pi\nu)^{-1}$ at $\nu = \chi_{M''max}$) at a given temperature are plotted as ln(τ) vs 1/T (Figure S11). It was found that the relaxation follows a thermally activated mechanism, with plots of ln(τ) vs 1/T being linear. These data were fitted to the Arrhenius law [$\tau = \tau_o \exp(U_{eff}/k_BT)$], which allowed for the evaluation of the anisotropy barrier (U_{eff}) and pre-exponential factor (τ_o), yielding an effective barrier to magnetization reversal of U_{eff} = 10.1 ± 0.6 K with $\tau_o = 9.9 \times 10^{-7}$ s (R = 0.99).

The resulting lack of SMM behavior in zero dc field for the Tb^{III}-containing complexes is now a common observation. The reason for this is due to the low symmetry found at the metal ion sites, and as a consequence, fast quantum tunneling relaxation pathways become active, due to the non-Kramers nature of the ion. Application of a magnetic field can reduce the tunneling relaxation time, and indeed a nonzero out-of-phase component is observed for $\{Cu^{II}_2Tb^{III}_7\}$ (**5**) under the application of a static dc field of 1500 Oe (Figure S12).

dx.doi.org/10.1021/ic5023467 | Inorg. Chem. 2014, 53, 13154−13161

CONCLUSIONS

In summary, by using copper and lanthanide chloride salts, in conjunction with triethanolamine and carboxylate ligands we have obtained two distinct 3d-4f heterometallic families that are structurally related. Using benzoic acid we can isolate compounds of core type $\{Cu_2Ln_7\}$, while using the more sterically demanding 2-biphenylcarboxylic acid ligand, compounds of core type $\{Cu_4Ln_{12}\}$ are isolated (Ln = Gd, Tb, and Dy). These polynuclear complex families both possess vertex-sharing cubane Ln^{III} metal topologies, with the Cu^{II} ions acting as "caps". The {Cu−Gd} compounds **1** and **4** display a huge MCE at low temperatures, with maximum entropy changes of 34.6 J kg^{-1} K^{-1} at T = 2.7 K and $-\Delta S_m$ = 33.0 J kg^{-1} K^{-1} ($\mu_0\Delta H$ = 9−0 T), respectively, the highest reported for any 0D polynuclear Cu−Gd system. The anisotropic $Cu-Dy^{III}$ analogues display SMM behavior in a zero static dc magnetic field, albeit with small anisotropy barriers.

ASSOCIATED CONTENT

Supporting Information

Crystallographic data in CIF format; Table S1, crystallographic data; Figures S1 and S2, packing diagrams; Figures S2−S7, dc magnetic data; Figures S8−S12, ac magnetic data. This material is available free of charge via the Internet at http://pubs.acs.org.

AUTHOR INFORMATION

Corresponding Authors

*E-mail: evange@unizar.es.

*E-mail: keith.murray@monash.edu.

Notes

The authors declare no competing financial interest.

ACKNOWLEDGMENTS

K.S.M. thanks the Australian Research Council (ARC) and the Australia-India Strategic Research Fund (AISRF) for support of this work. M.E. acknowledges financial support from MINECO through grant MAT2012-38318-C03-01. Part of this research was undertaken on the MX1 beamline at the Australian Synchrotron, Victoria, Australia.

REFERENCES

(1) (a) Murray, K. S. *Aust. J. Chem.* **2009**, *62*, 1081−1101. (b) Gatteschi, D.; Sessoli, R.; Villain, J. *Molecular Nanomagnets*; Oxford University Press: Oxford, 2006.

(2) (a) Christou, G.; Gatteschi, D.; Hendrikson, D. N.; Sessoli, R. *MRS Bull.* **2000**, 66−71. (b) Aromí, G.; Brechin, E. K. *Struct. Bonding (Berlin)* **2006**, *122*, 1−67. (c) Zhang, P.; Guo, Y.-N.; Tang, J. *Coord. Chem. Rev.* **2013**, *257*, 1728−1763. (d) Ungur, L.; Lin, S.-Y.; Tang, J.; Chibotaru, L. *Chem. Soc. Rev.* **2014**, *43*, 6894−6905. (e) Leuenberger, M. N.; Loss, D. *Nature* **2001**, *410*, 789−793.

(3) (a) Evangelisti, M.; Brechin, E. K. *Dalton Trans.* **2010**, *39*, 4672−4676. (b) Evangelisti, M.; Luis, F.; de Jongh, J. L.; Affronte, M. *J. Mater. Chem.* **2006**, *16*, 2534−2549. (c) Sessoli, R. *Angew. Chem., Int. Ed.* **2012**, *51*, 43−45. (d) Evangelisti, M. In *Molecular Magnets, NanoScience and Technology*; Bartolomé, J.; Luis, F.; Fernández, J. F., Eds.; Springer-Verlag: Berlin, 2014; pp 365−387.

(4) (a) Woodruff, D. N.; Layfield, R. A.; Winpenny, R. E. P. *Chem. Soc. Rev.* **2013**, *113*, 5110−5148. (b) Rhinehart, J. D.; Fang, M.; Evans, W. J.; Long, J. R. *J. Am. Chem. Soc.* **2011**, *133*, 14236−14239. (c) Rhinehart, J. D.; Fang, M.; Evans, W. J.; Long, J. R. *Nat. Chem.* **2011**, *3*, 538−542. (d) Rhinehart, J. D.; Fang, M.; Evans, W. J.; Long, J. R. *J. Am. Chem. Soc.* **2011**, *133*, 14236−14239. (e) Blagg, R. J.; Ungur, L.; Tuna, F.; Speak, J.; Comar, P.; Collison, D.; Wernsdorfer, W.; McInnes, E. J. L.; Chibotaru, L. F.; Winpenny, R. E. P. *Nat. Chem.* **2013**, *5*, 673−678. (f) Le Roy, J. J.; Korobkov, I.; Murugesu, M. *Chem. Commun.* **2014**, *50*, 1602−1604. (g) Ganivet, C. R.; Ballesteros, B.; de la Torre, G.; Clemente-Juan, J. M.; Coronado, E.; Torres, T. *Chem.—Eur. J.* **2013**, *19*, 1457−1465. (h) Zhang, P.; Zhang, L.; Wang, C.; Xue, S.; Lin, S.-L.; Tang, J. *J. Am. Chem. Soc.* **2014**, *136*, 4484−4487.

(5) For example: (a) Zheng, Y.-Z.; Zhou, G.-J.; Zheng, Z.; Winpenny, R. E. P. *Chem. Soc. Rev.* **2014**, *43*, 1462−1475. (b) Evangelisti, M.; Roubeau, O.; Palacios, E.; Camón, A.; Hooper, T. N.; Brechin, E. K.; Alonso, J. J. *Angew. Chem., Int. Ed.* **2011**, *50*, 6606−6609. (c) Sibille, R.; Mazet, T.; Malaman, B.; Francois, M. *Chem.—Eur. J.* **2012**, *18*, 12970−12973. (d) Chang, L.-X.; Xiong, G.; Wang, L.; Cheng, P.; Zhao, B. *Chem. Commun.* **2013**, *49*, 1055−1057. (e) Evangelisti, M.; Luis, F. *Struct. Bonding (Berlin)* **2014**, DOI: 10.1007/430_2014_152.

(6) Lorusso, G.; Sharples, J. W.; Palacios, E.; Roubeau, O.; Brechin, E. K.; Sessoli, R.; Rossin, A.; Tuna, F.; McInnes, E. J. L.; Collison, D.; Evangelisti, M. *Adv. Mater.* **2013**, *25*, 4653−4656.

(7) (a) Bencini, A.; Benelli, C.; Caneschi, A.; Carlin, R.; Dei, A.; Gatteschi, D. *J. Am. Chem. Soc.* **1985**, *107*, 8128−8136. (b) Andruh, M.; Ramade, I.; Codjovi, E.; Guillou, O.; Kahn, O.; Trombe, J. C. *J. Am. Chem. Soc.* **1993**, *115*, 1822−1829. (c) Benelli, C.; Gatteschi, D. *Chem. Rev.* **2002**, *102*, 2369−2388. (d) Kahn, M. L.; Mathoniere, C.; Kahn, O. *Inorg. Chem.* **1999**, *38*, 3692−3697.

(8) Langley, S. K.; Chilton, N. F.; Moubaraki, B.; Hooper, T.; Brechin, E. K.; Evangelisti, M.; Murray, K. S. *Chem. Sci.* **2011**, *2*, 1166−1169.

(9) Langley, S. K.; Ungur, L.; Chilton, N. F.; Moubaraki, B.; Chibotaru, L. F.; Murray, K. S. *Chem.—Eur. J.* **2011**, *17*, 9209−9218.

(10) (a) Langley, S. K.; Moubaraki, B.; Berry, K. J.; Murray, K. S. *Dalton Trans.* **2010**, *40*, 4848−4855. (b) Langley, S. K.; Chilton, N. F.; Moubaraki, B.; Murray, K. S. *Dalton Trans.* **2011**, *39*, 12201−12209. (c) Langley, S. K.; Chilton, N. F.; Moubaraki, B.; Murray, K. S. *Dalton Trans.* **2012**, *41*, 9789−9796. (d) Langley, S. K.; Chilton, N. F.; Ungur, L.; Moubaraki, B.; Chibotaru, L. F.; Murray, K. S. *Inorg. Chem.* **2012**, *51*, 11873−11881. (e) Langley, S. K.; Chilton, N. F.; Moubaraki, B.; Murray, K. S. *Inorg. Chem.* **2013**, *52*, 7183−7192. (f) Ungur, L.; Langley, S. K.; Hooper, T. N.; Moubaraki, B.; Brechin, E. K.; Murray, K. S.; Chibotaru, L. F. *J. Am. Chem. Soc.* **2012**, *134*, 18554−18557.

(11) Winpenny, R. E. P. *J. Chem. Soc., Dalton Trans.* **2002**, 1−10.

(12) McPhillips, T. M.; McPhillips, S. E.; Chiu, H. J.; Cohen, A. E.; Deacon, A. M.; Ellis, P. J.; Garman, E.; Gonzalez, A.; Sauter, N. K.; Phizackerley, R. P.; Soltis, S. M.; Kuhn, P. *J. Synchrotron Radiat.* **2002**, *9*, 401−406.

(13) Kabsch, W. *J. Appl. Crystallogr.* **1993**, *26*, 795−800.

(14) Sheldrick, G. M. *Acta Crystallogr. A* **2008**, *A64*, 112−122.

(15) (a) Graham, A.; Meier, S.; Parsons, S.; Winpenny, R. E. P. *Chem. Commun.* **2000**, 811−812. (b) Sharples, J. W.; Zheng, Y.-Z.; Tuna, F.; McInnes, E. J. L.; Collison, D. *Chem. Commun.* **2011**, *47*, 7650−7652. (c) Langley, S. K.; Helliwell, M.; Teat, S. J.; Winpenny, R. E. P. *Dalton Trans.* **2012**, *41*, 12807−12817.

(16) Hooper, T. N.; Schnack, J.; Piligkos, S.; Evangelisti, M.; Brechin, E. K. *Angew. Chem., Int. Ed.* **2012**, *51*, 4633−4636.

(17) (a) Leng, J.-D.; Liu, J.-L.; Tong, M.-L. *Chem. Commun.* **2012**, *48*, 5286−5288. (b) Liu, J. L.; Chen, Y.-C.; Li, Q.-W.; Gomez-Coca, S.; Aravena, D.; Ruiz, E.; Lin, W.-Q.; Leng, J.-D.; Tong, M.-L. *Chem. Commun.* **2013**, *49*, 6549−6551. (c) Dinca, A. S.; Ghirri, A.; Madalan, A. M.; Affronte, M.; Andruh, M. *Inorg. Chem.* **2012**, *51*, 3953−3955. (d) Xue, S.; Guo, Y.-N.; Zhao, L.; Zhang, H.; Tang, J. *Inorg. Chem.* **2014**, *53*, 8165−8171.

(18) Peng, J. B.; Zhang, Q. C.; Kong, X. J.; Zheng, Y. Z.; Ren, Y. P.; Long, L. S.; Huang, R. B.; Zheng, L. S.; Zheng, Z. *J. Am. Chem. Soc.* **2012**, *134*, 3314−3317.

(19) Peng, J. B.; Zhang, Q. C.; Kong, X. J.; Ren, Y. P.; Long, L. S.; Huang, R. B.; Zheng, L. S.; Zheng, Z. *Angew. Chem., Int. Ed.* **2011**, *50*, 10649−10652.